Iraqi J. Laser, issue 2, vol., 20, pp. 32-41 (2021)

IRAQI JOURNAL OF LASER

On the use of Aluminium as a plasmonic material in polarization rotators based on a hybrid plasmonic waveguide

Farooq Abdulghafoor Khaleel[1,*], Shelan Khasro Tawfeeq[1]

**Corresponding author: farook.abd1101a@ilps.uobaghdad.edu.iq*

1. Institute of Laser for Postgraduate Studies, University of Baghdad, Iraq, Baghdad, Iraq.

(Received 21/11/2021; accepted 29/12/2021)

Abstract: The Aluminium (Al) material emerged as a plasmonic material in the wavelength ranges from the ultraviolet to the visible bands in different on-chip plasmonic applications. In this paper, we demonstrate the effect of using Al on the electromagnetic (EM) field distribution of a compact hybrid plasmonic waveguide (HPW) acting as a polarization rotator. We compare the performance of Al with other familiar metals that are widely used as plasmonic materials, which are Silver (Ag) and Gold (Au). Furthermore, we study the effect of reducing the geometrical dimensions of the used materials on the EM field distributions inside the HPW and, consequently, on the efficiency of the polarization rotation. We perform the study based on the Finite Element Method (FEM) using COMSOL software at an operation wavelength of 700 nm. This paper verifies that the Al could be used as an efficient plasmonic material in integrated single-photon sources for quantum key distribution systems.

Key words:

1. Introduction

The photonic applications at the visible and infrared wavelengths depend widely on plasmonics. Recent researches showed considerable progress in plasmon-based light trapping [1, 2], surface-enhanced spectroscopy [3, 4], sensors [5, 6], optoelectronic devices [7, 8], nonlinear optics [9, 10], and photocatalysis [11, 12]. In nanoscale devices, extending the plasmonic excitation effect from infrared, visible to the ultraviolet wavelengths range is a major challenge. The challenge arises from the limited performance (i.e. weak resonance effect) of the common plasmonic metals, which are Au and Ag, at the visible and UV wavelengths ranges [13, 14]. The Ag exhibited rapid oxidation that deteriorates the plasmonic effects, while the interband transitions in Au increase at the visible wavelength ranges and below and act as a dissipative channel that weakens the plasmonic effect [15, 16]. However, the Al emerged as a preferable plasmonic metal at the visible and UV wavelengths because of its strong resonance at these wavelengths, natural availability, low cost, and fabrication easiness and accuracy down to 5 nm linewidth [17, 18].

One of the most important integrated plasmonic devices is the polarization rotators [19]. Recently, the polarization rotators are applied in integrated single-photon sources in polarization-based quantum key distribution systems [20]. The aim of [20] was to control the output polarization of the emitted photons from a quantum emitter (QE) coupled to an HPW acting as a polarization rotator. Moreover, the emission wavelength of most QEs is 700 nm, where the Au and Ag plasmonic metals begin to lose their plasmonics properties [21].

This paper compares the performance of using Au, Ag, and Al as plasmonic metals in polarization rotators based on HPW. Furthermore, the effect of using different plasmonic metals on the miniaturization of the integrated HPW will also be discussed. This paper is arranged as follows: Section (2) demonstrates the principles of the polarization rotators. Section (3) compares the performance of the polarization rotator using different plasmonics metals. Finally, Section (4) concludes our findings.

2. The principles of integrated polarization rotators

In general, the HPW at the telecommunication wavelengths (1.3 or 1.55) µm is composed of a thin dielectric spacer of low refractive index (silica (SiO_2)) that separates a high refractive index medium (silicon (Si)) from a metal conductor (gold (Au) or silver (Ag)) as shown in figure (1).

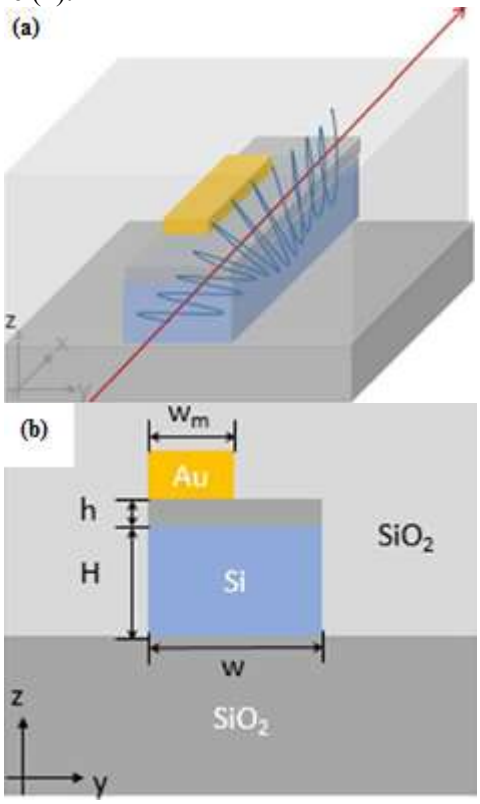

Figure (1): The general structure of an HPW at a wavelength of 1.55 µm, (a) A 3D view, (b) A 2D cross-section [22]

The HPW propagation modes are a combination of the photonic modes supported by the high refractive index medium (i.e. photonic waveguide) and the SPP modes at the metal-dielectric boundary (i.e. PW). The HPW combines two features— the small losses feature exhibited by a photonic waveguide and the high light confinement feature exhibited by the PW [22]. The HPW is selected as a basis for polarization rotators because of its structure and features.

Figure (1. a) presents how the HPW can perform as an integrated linear polarization rotator. Figure (1. b) shows the rotator's cross-section, which shows that the metal has a reduced width than the Si and SiO_2 layers forming an asymmetric HPW [22]. The asymmetry structure destroys the horizontal symmetry in the Si and, consequently, rotates the optical axes of the supported propagation eigenmodes. Therefore, the asymmetric HPW supports two orthogonal propagation modes rotated by an optical axis angle (θ), which is defined by [23]:

$$tan(\theta) = \iint \frac{\epsilon(y,z)E_y^2(y,z)dydz}{\epsilon(y,z)E_z^2(y,z)dydz} \dots\dots\dots\dots (1)$$

Where $\epsilon(y,z)$ is the real part of the permittivity distribution in the (y-z) plane, and E_z and E_y are the horizontal and transversal electric field distribution of the propagation mode, respectively. The resulting two orthogonal propagation modes for the polarization rotator presented in Figure (1) are shown in Figure (2) for different Au widths (w_m) [22]:

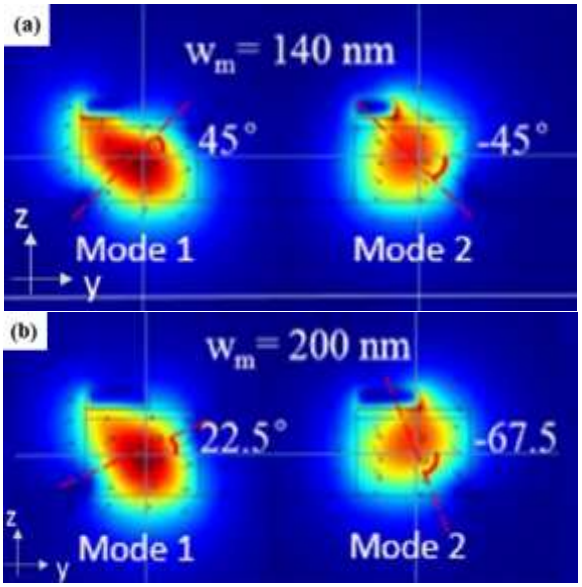

Figure (2): The magnetic field distribution of the two orthogonal propagation modes for an Au width of (a) 140 nm and (b) 200 nm resulting in θ of 45º and 22.5º, respectively [22]

The Au's width varies the angle of the optical axis of the propagation mode, and consequently, the output polarization. Moreover, the Au's length (L) identifies the difference between the phase (δ) of the two propagation modes in the metal part, which are related by [23]:

$$\delta = \frac{2\pi L}{\lambda}|n_1 - n_2| \dots\dots\dots\dots\dots\dots\dots\dots\dots\dots\dots (2)$$

Where n_1 and n_2 are the real parts of the effective indices of the two orthogonal propagation modes, and λ is the wavelength. Consequently, by selecting a certain metal length and width, the rotator can perform as λ/4 or λ/2 waveplate. The polarization rotator

proposed in [23] operates efficiently at a 1550 nm wavelength. However, it is a challenge to find a metal that preserves the orthogonality of the propagation modes at 700 nm. Such a metal is required in polarization rotators that control the emission polarization of an embedded QE inside the HPW. Besides, alternative materials to Si and SiO_2 should be chosen to support the light's propagation at 700 nm. Table (1) shows the n and κ for different materials, where n is the real part of the material's refractive index that determines the light's phase velocity and κ is the imaginary part of the material's refractive index that determines the attenuation coefficient.

The Si material shows a considerable value of κ at 700 nm and, hence, the light propagating in the Si material is significantly attenuated as Beer-Lambert law implies. Recently, gallium phosphide (GaP) played an important role in many modern photonic integrated circuits (PICs) [26]. GaP supports strong light confinement and small mode volume due to its high refractive index at 700 nm [27]. Consequently, the alternative material at 700 nm that shows a comparable refractive index for the Si at 1550 nm is the GaP as shown in Table (1).

Moreover, the SiO_2 and the hydrogen silsesquioxane (HSQ) materials show a comparable refractive index at a wide range of wavelengths as shown in Table (1). However, the HSQ material is selected as a basis for the 700 nm HPW because it is a widely used material in on-chip plasmonic single-photon sources and it could be experimentally converted to SiO_2 with the same performance [21, 28]. The reasons for choosing the Al as a plasmonic material include its strong plasmonic resonance, simple manufacturing processes, and low cost [29]. The Al could be fabricated down to a 5 nm scale, which makes it easily handled during the manufacturing process [17, 18]. Both gold and silver exhibit high plasma wavelength and, therefore, weak plasmonic resonance in contrast to Al at 700 nm. Although the Au and Ag have approximately comparable refractive indices as shown in Table (1), Au and Ag failed to achieve the polarization rotation at a wavelength of 700 nm because of the real part n's deterioration.

Table (1): The refractive indices information for different materials [24]

Material	n	κ	n	κ	n	κ	The model
	@ 700 nm		@ 1.3 µm		@ 1.55 µm		
Si	4.0679	0.25109	3.5226	0	3.48	0	Pierce and Spicer
SiO_2	1.4553	0	1.4469	0	1.444	0	Malitson
Au	0.131	4.0624	0.38797	8.7971	0.52406	10.742	Johnson and Christy
Ag	0.041	4.8025	0.10898	9.4317	0.14447	11.366	Johnson and Christy
GaP	3.2992	0	3.1447	0	3.128	0	Adachi
HSQ	1.41	0	1.41	0	1.41	0	Dow Corning® XR-1541 E-Beam Resist [25]
Al	1.9214	8.142	1.3481	12.917	1.5785	15.658	Rakić

3. Simulation results

The polarization rotation requires that the GaP photonic waveguide supports two orthogonal propagation modes for each case of output polarization, which was achieved by using Al (strong plasmonic resonance) instead of Au and Ag (weak plasmonic resonance) as shown in Figure (3) for 0°, 90°, 45°, and -45° output polarization cases. In the following simulations,

the refractive index information for Al and GaP are based on RakiA and Aspnes and Studna models, respectively, that are defined in the COMSOL's material library. Consequently, the refractive indices for the Al and GaP are 1.9214 + 8.142i and 3.2543 at 700 nm, respectively. Figure (3) shows that there exist two orthogonal modes, for each case of output polarization, supported by the HPW at optimum dimensions.

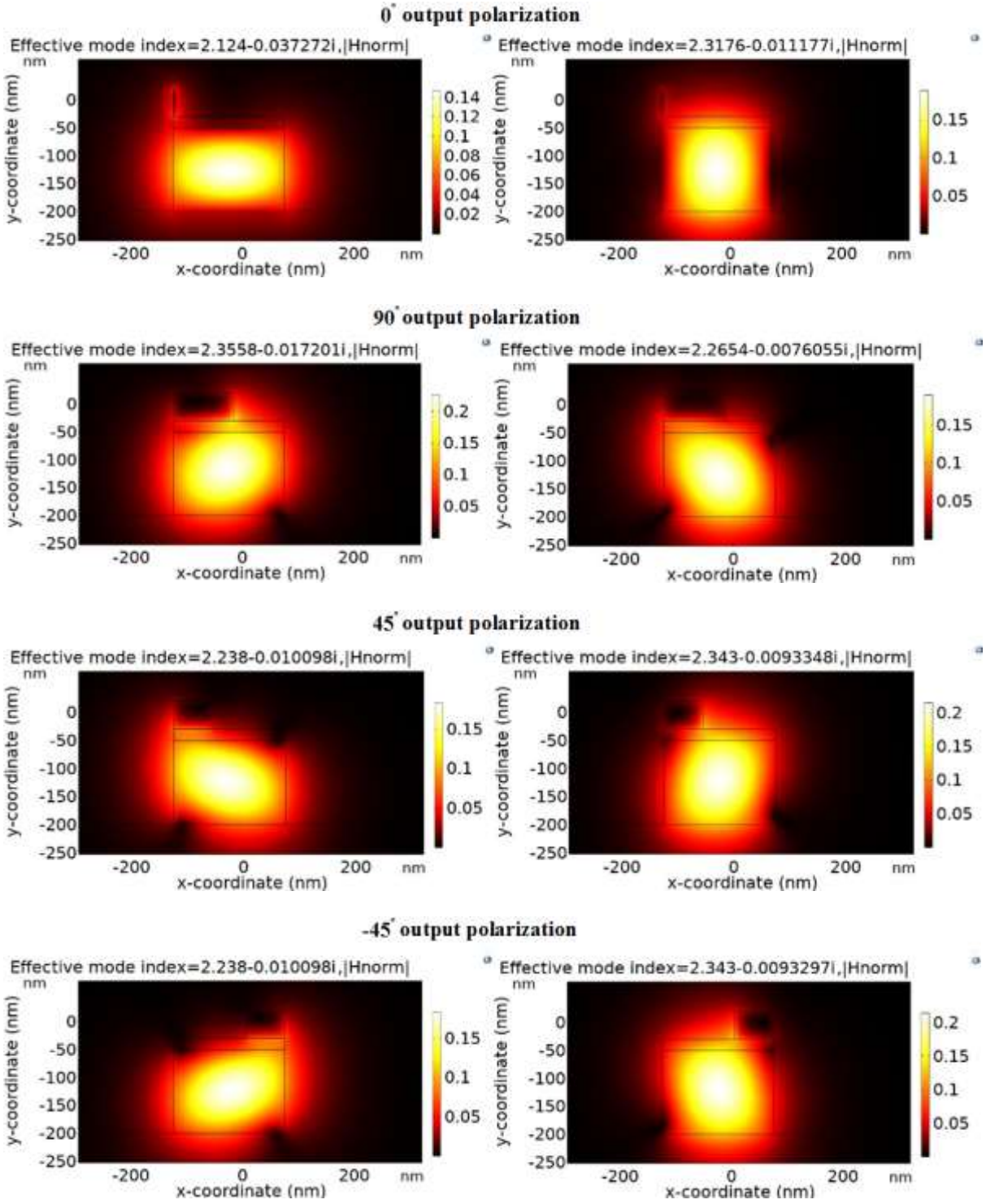

Figure (3): The two orthogonal modes supported by the HPW for each case of output polarization for Al material at 700 nm

However, the propagation modes lose their orthogonality if an Au or Ag metal is used instead of the Al metal (at the same optimum dimensions) as shown in figure (4).

Au , 0°, output polarization

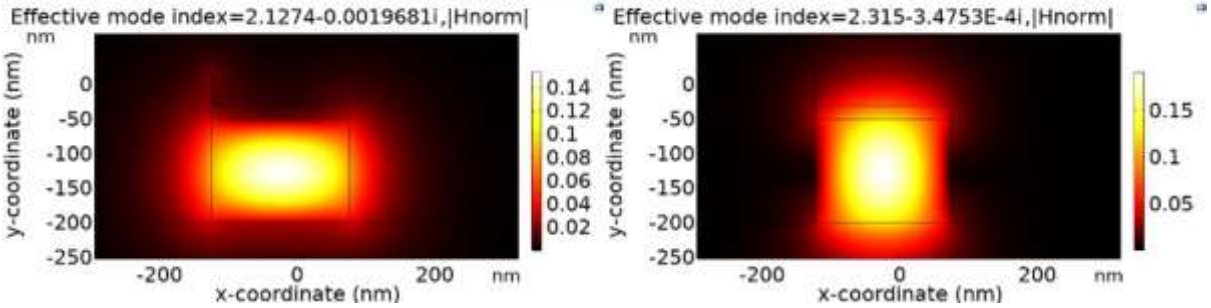

Au , 90°, output polarization

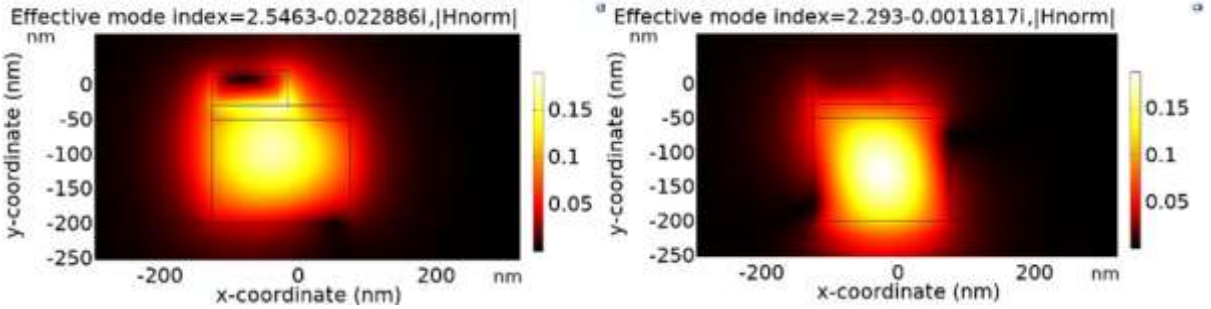

Au , 45°, output polarization

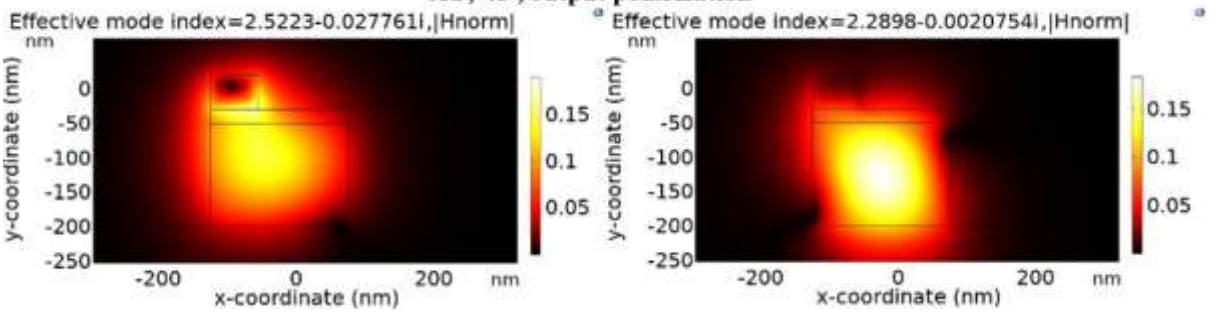

Au , -45°, output polarization

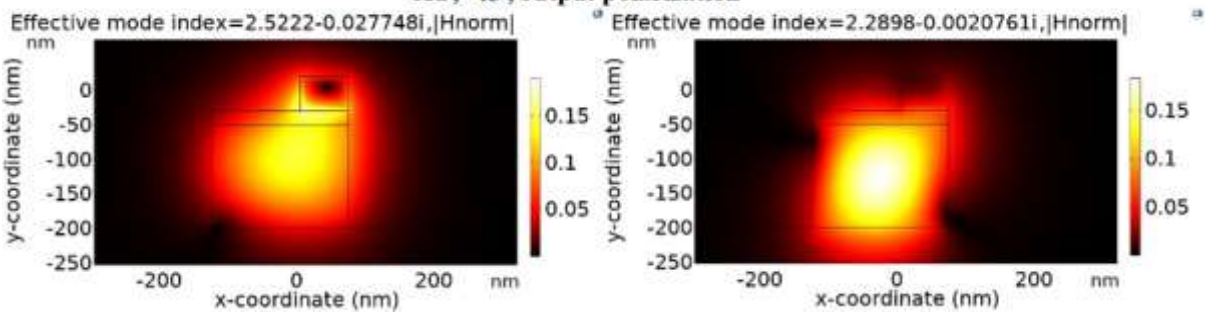

Ag , 0°, output polarization

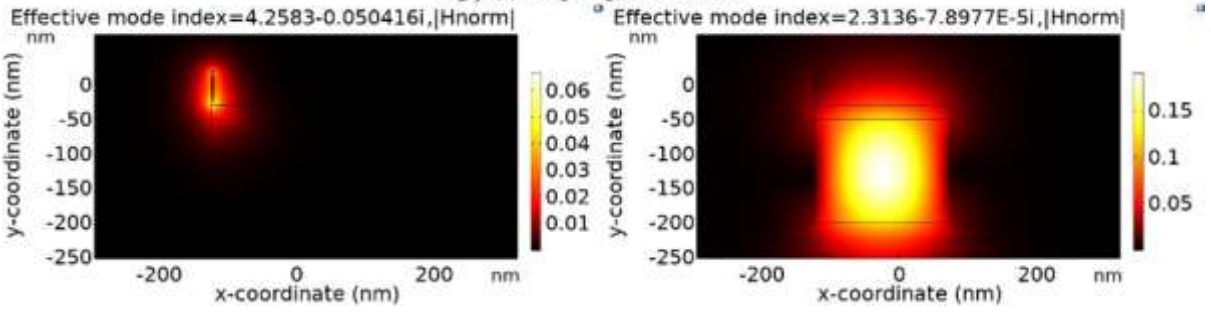

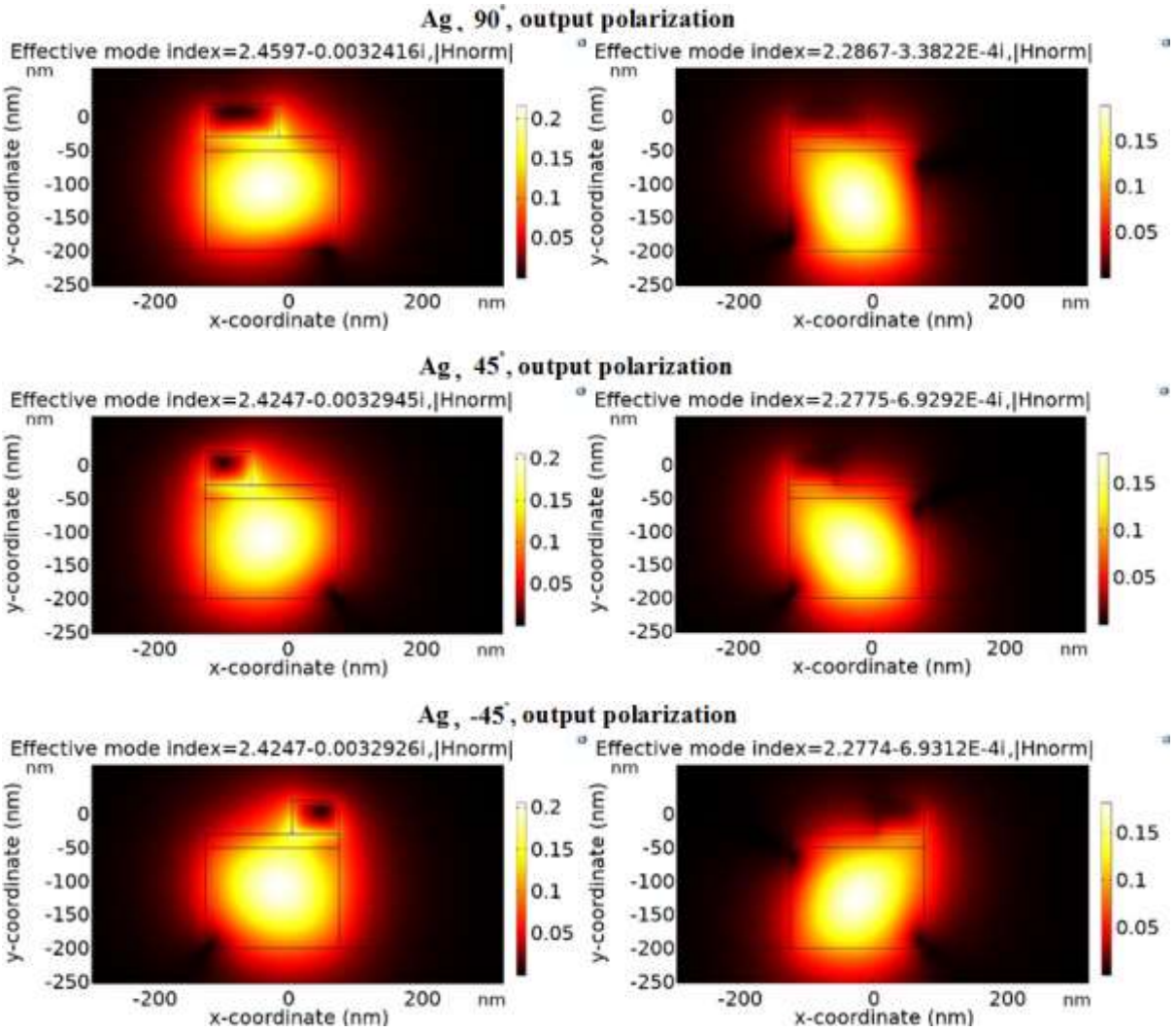

Figure (4): The two orthogonal modes supported by the HPW for each case of output polarization when Au and Ag metals are used at 700 nm.

On another hand, a mandatory requirement to control the output polarization of the HPW is that the HPW's geometrical dimensions should support the propagation of two orthogonal modes. The dimensions of the HPW are determined by the local search algorithm. Most of the on-chip plasmonic single-photon sources used 250 nm (width) and 180 nm (height) for the HSQ pattern deposited above silver or gold as shown in figure (5) [21,28,30].

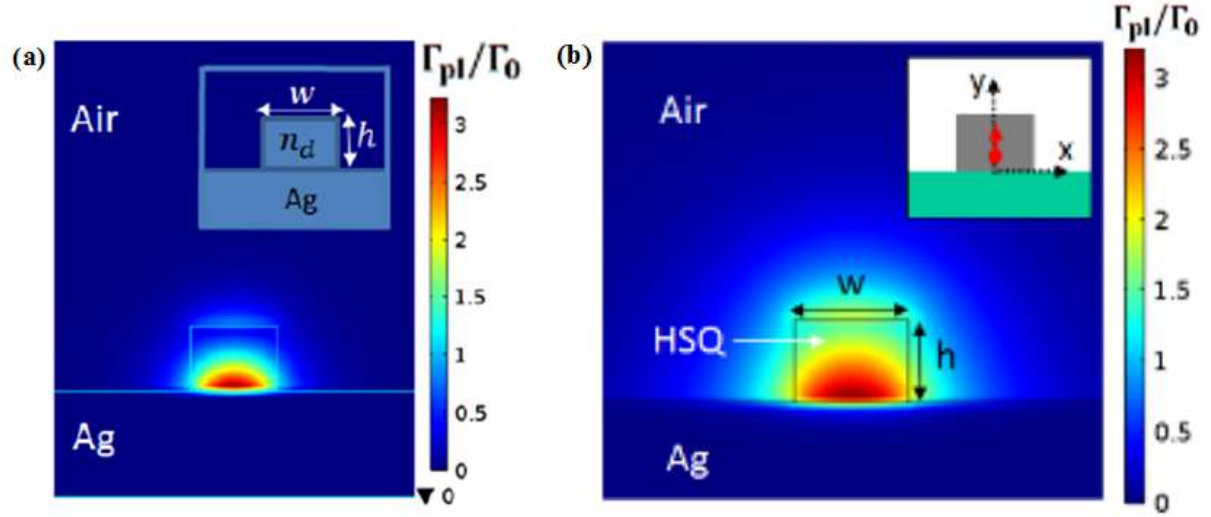

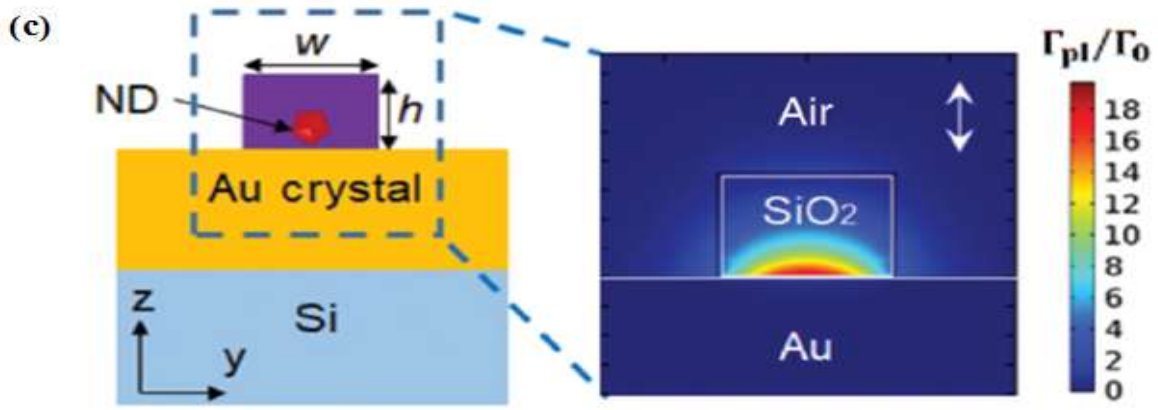

Figure (5): The HSQ's geometries in DLSPP waveguides used as on-chip plasmonic single-photon sources. (a) [21], (b) [30], (c) [28]

The 250 nm (width) and 180 nm (height) dimensions were considered as a reference to select the GaP photonic channel dimensions in the HPW, which achieved the orthogonality of the propagation modes condition in the GaP region as shown in Figure (6. a,b). However, the proposed work tends to miniaturize the dimensions of the HPW to save space on the integrated circuit. Hence, the width and the height of the GaP photonic waveguides decreased while keeping the Al bar and the HSQ spacer heights fixed at 50 nm and 20 nm, respectively. The minimum dimensions of the GaP region that supports the propagation of two orthogonal modes are 200 nm (width) and 150 nm (Height) as shown in Figure (6. c,d). The propagation modes lose their orthogonality if the GaP's width or height is reduced to 190 nm or 145 nm, respectively, as shown in Figure (6. e-h).

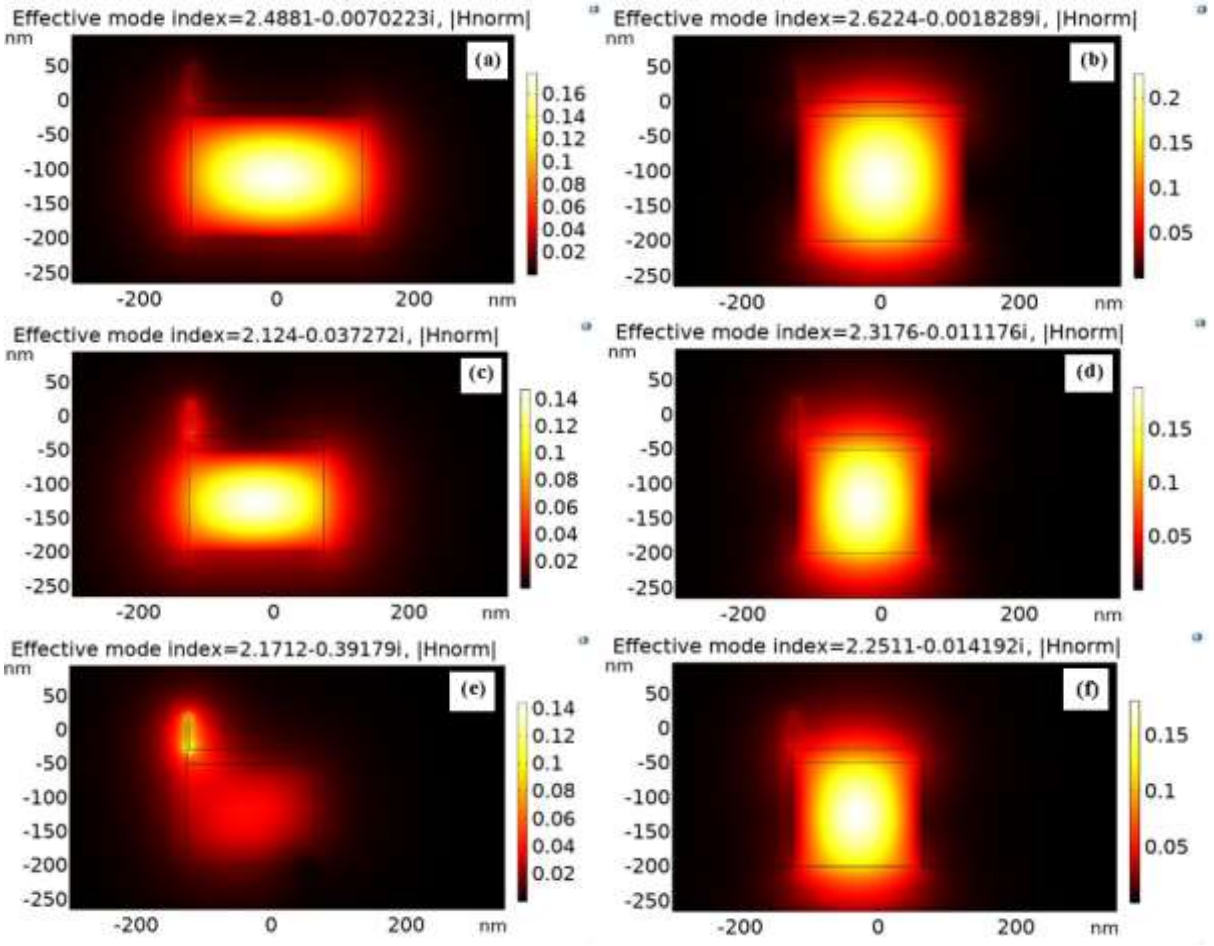

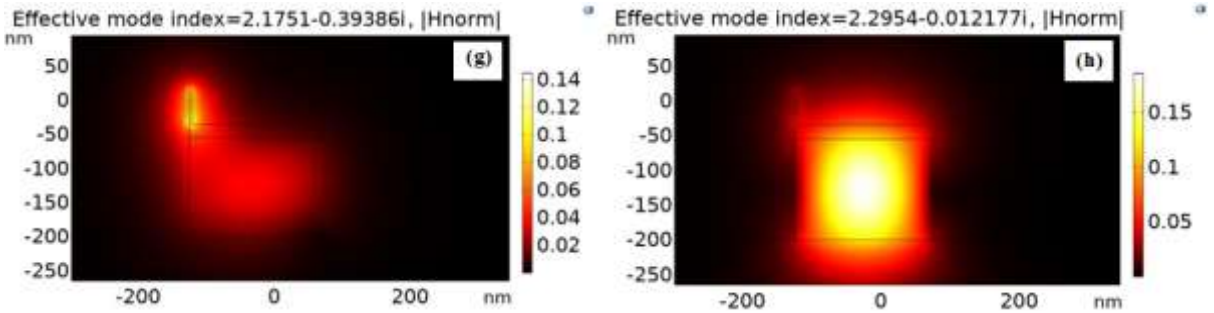

Figure (6): The orthogonal modes field distribution when the width and height of the GaP region is (a), (b) 250, 180 nm, (c), (d) 200, 150 nm, (e), (f) 190, 150 nm, and (g), (h) 200, 145 nm, respectively.

The HSQ spacer covers the GaP and, consequently, has the same width as the GaP layer. However, the HSQ spacer's height and the Al bar's width affect the mechanism of the polarization control technique, and, consequently, their optimum values are justified in [20]. Finally, the Al metal height affects the orthogonality of the propagation modes. If the Al metal bar height is set to 45 nm, the orthogonality is lost as shown in figure (7. a,b). Consequently, the minimum Al bar's height that enables the GaP region to support the propagation of two orthogonal modes is 50 nm as shown in figure (7. c,d).

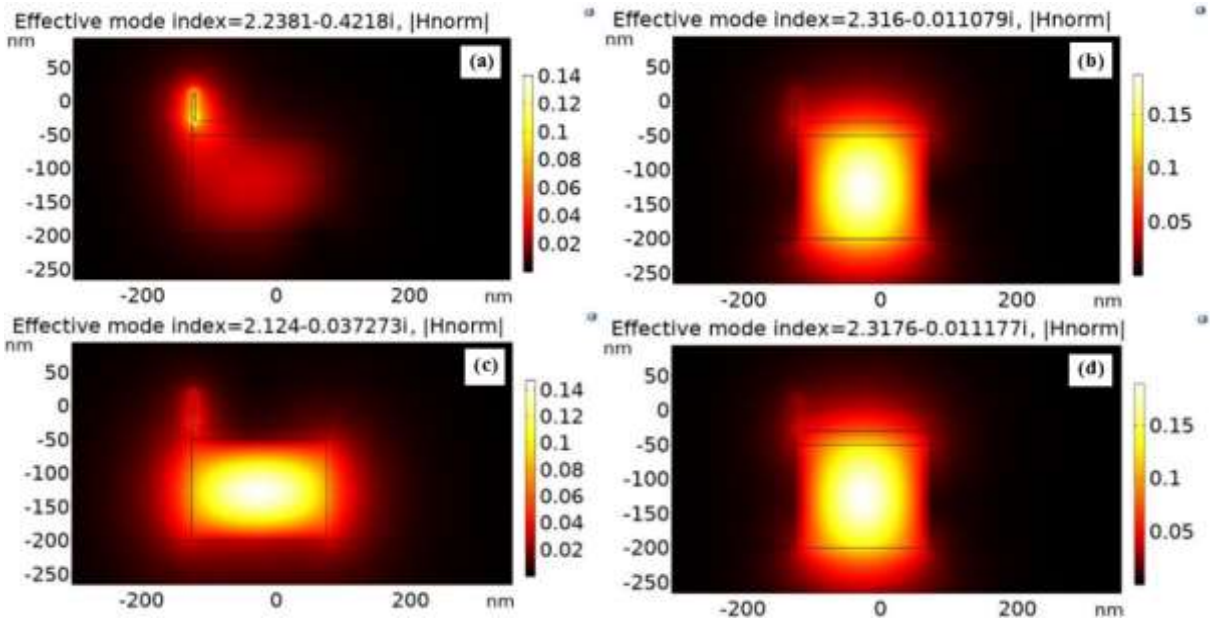

Figure (7): The orthogonal modes field distribution with Al bar's height of (a), (b) 45 nm, and (c), (d) 50 nm.

4. Conclusions

The Al metal proved to be an efficient plasmonic material for 700 nm wavelength plasmonic applications in comparison to Au or Ag. The Al succeeded in preserving the orthogonality of the propagation modes for the HPW with minimum possible geometrical dimensions. Other metals could be investigated for different plasmonic applications at the visible and UV wavelengths range such as copper, lead, etc. Moreover, the compactness of the plasmonic polarization rotator has its unique geometrical limitations. Different PW topologies could be further investigated in the future for further miniaturization of the plasmonic circuit at the visible or UV wavelengths range.

5. References

[1] T.F. Villesen, C. Uhrenfeldt, B. Johansen, A.N. Larsen, Self-assembled Al nanoparticles on Si and fused silica, and their application for Si solar cells, Nanotechnology. 24 (2013).

[2] T.F. Villesen, C. Uhrenfeldt, B. Johansen, J.L. Hansen, H.U. Ulriksen, A.N. Larsen, Aluminum nanoparticles for plasmon-improved coupling of light into silicon, Nanotechnology. 23 (2012).

[3] C. D'Andrea, J. Bochterle, A. Toma, C. Huck, F. Neubrech, E. Messina, B. Fazio, O.M. Maragò, E. Di Fabrizio, M. Lamy de La Chapelle, P.G. Gucciardi, A. Pucci, Optical Nanoantennas for Multiband Surface-Enhanced Infrared and Raman Spectroscopy, ACS Nano. 7 (2013).
[4] Y. Zheng, T. Thai, P. Reineck, L. Qiu, Y. Guo, U. Bach, DNA-Directed Self-Assembly of Core-Satellite Plasmonic Nanostructures: A Highly Sensitive and Reproducible Near-IR SERS Sensor, Adv. Funct. Mater. 23 (2013).
[5] N. Mattiucci, G. D'Aguanno, H.O. Everitt, J. V Foreman, J.M. Callahan, M.C. Buncick, M.J. Bloemer, Ultraviolet surface-enhanced Raman scattering at the plasmonic band edge of a metallic grating, Opt. Express. 20 (2012).
[6] A. Ono, M. Kikawada, R. Akimoto, W. Inami, Y. Kawata, Fluorescence enhancement with deep-ultraviolet surface plasmon excitation, Opt. Express. 21 (2013).
[7] H. Zhang, J. Zhou, W. Zou, M. He, Surface plasmon amplification characteristics of an active three-layer nanoshell-based spaser, J. Appl. Phys. 112 (2012).
[8] Y. Chen, G. Song, J. Xiao, L. Yu, J. Zhang, Subwavelength polarization beam splitter with controllable splitting ratio based on surface plasmon polaritons, Opt. Express. 21 (2013).
[9] A. Grubisic, V. Schweikhard, T.A. Baker, D.J. Nesbitt, Coherent Multiphoton Photoelectron Emission from Single Au Nanorods: The Critical Role of Plasmonic Electric Near-Field Enhancement, ACS Nano. 7 (2013).
[10] G.F. Walsh, L. Dal Negro, Enhanced Second Harmonic Generation by Photonic–Plasmonic Fano-Type Coupling in Nanoplasmonic Arrays, Nano Lett. 13 (2013).
[11] S. Mukherjee, F. Libisch, N. Large, O. Neumann, L. V Brown, J. Cheng, J.B. Lassiter, E.A. Carter, P. Nordlander, N.J. Halas, Hot Electrons Do the Impossible: Plasmon-Induced Dissociation of H2 on Au, Nano Lett. 13 (2013).
[12] A.O. Govorov, H. Zhang, Y.K. Gun'ko, Theory of Photoinjection of Hot Plasmonic Carriers from Metal Nanostructures into Semiconductors and Surface Molecules, J. Phys. Chem. C. 117 (2013).
[13] J.M. McMahon, G.C. Schatz, S.K. Gray, Plasmonics in the ultraviolet with the poor metals Al, Ga, In, Sn, Tl, Pb, and Bi, Phys. Chem. Chem. Phys. (Incorporating Faraday Trans. 15 (2013).
[14] G. V Naik, V.M. Shalaev, A. Boltasseva, Alternative Plasmonic Materials: Beyond Gold and Silver, Adv. Mater. 25 (2013).
[15] A. Taguchi, Y. Saito, K. Watanabe, S. Yijian, S. Kawata, Tailoring plasmon resonances in the deep-ultraviolet by size-tunable fabrication of aluminum nanostructures, Appl. Phys. Lett. 101 (2012).
[16] G. Maidecchi, G. Gonella, R. Proietti Zaccaria, R. Moroni, L. Anghinolfi, A. Giglia, S. Nannarone, L. Mattera, H.-L. Dai, M. Canepa, F. Bisio, Deep Ultraviolet Plasmon Resonance in Aluminum Nanoparticle Arrays, ACS Nano. 7 (2013).
[17] M. Kjaergaard, F. Nichele, H.J. Suominen, M.P. Nowak, M. Wimmer, A.R. Akhmerov, J.A. Folk, K. Flensberg, J. Shabani, C.J. Palmstrøm, C.M. Marcus, Quantized conductance doubling and hard gap in a two-dimensional semiconductor–superconductor heterostructure, Nat. Commun. 7 (2016).
[18] T. Morgan-Wall, H.J. Hughes, N. Hartman, T.M. McQueen, N. Marković, Fabrication of sub-15 nm aluminum wires by controlled etching, Appl. Phys. Lett. 104 (2014).
[19] F. Wang, Y. Chen, T. Ma, H. Liu, X. Wang, C. Jin, Mid-infrared polarization rotator based on a Si3N4-CaF2 hybrid plasmonic waveguide with asymmetric metal claddings, Appl. Opt. 60 (2021).
[20] F.A. Khaleel, S.K. Tawfeeq, The spontaneous emission performance of a quantum emitter coupled to a hybrid plasmonic waveguide with specified output polarization for on-chip plasmonic single-photon source, Photonics Nanostructures - Fundam. Appl. 45 (2021).
[21] H. Siampour, S. Kumar, S.I. Bozhevolnyi, Nanofabrication of Plasmonic Circuits Containing Single Photon Sources, ACS Photonics. (2017).
[22] L. Gao, Y. Huo, K. Zang, S. Paik, Y. Chen, J.S. Harris, Z. Zhou, On-chip plasmonic waveguide optical waveplate, Sci. Rep. 5 (2015).
[23] J.N. Caspers, M.Z. Alam, M. Mojahedi, Compact hybrid plasmonic polarization rotator, Opt. Lett. 37 (2012).

[24] Refractive index database, (n.d.). www.refractiveindex.info (accessed June 10, 2021).
[25] Dow Corning® XR-1541 E-Beam Resist, (2008).
[26] B. Tilmann, G. Grinblat, R. Berté, M. Özcan, V.F. Kunzelmann, B. Nickel, I.D. Sharp, E. Cortés, S.A. Maier, Y. Li, Nanostructured amorphous gallium phosphide on silica for nonlinear and ultrafast nanophotonics, Nanoscale Horiz. 5 (2020).
[27] K. Schneider, P. Welter, Y. Baumgartner, H. Hahn, L. Czornomaz, P. Seidler, Gallium Phosphide-on-Silicon Dioxide Photonic Devices, J. Light. Technol. 36 (2018).
[28] H. Siampour, O. Wang, V.A. Zenin, S. Boroviks, P. Siyushev, Y. Yang, V.A. Davydov, L.F. Kulikova, V.N. Agafonov, Ultrabright single-photon emission from germanium-vacancy zero-phonon lines : deterministic emitter-waveguide interfacing at plasmonic hot spots, Nanophotonics. (2020).
[29] M.W. Knight, N.S. King, L. Liu, H.O. Everitt, P. Nordlander, N.J. Halas, Aluminum for Plasmonics, ACS Nano. 8 (2014).
[30] H. Siampour, S. Kumar, S.I. Bozhevolnyi, Chip-integrated plasmonic cavity-enhanced single nitrogen- vacancy center emission, Nanoscale. (2017).

حول استخدام الالمنيوم كمادة بلازمونية في مدورات القطبية المبنية على الدليل الموجي الهجين

فاروق عبد الغفور خليل[1]* ، أ.م.د. شيلان خسرو توفيق[1]

[1]معهد الليزر للدراسات العليا – جامعة بغداد، بغداد - العراق

*Farook.abd1101a@ilps.uobaghdad.edu.iq

الخلاصة: ظهرت مادة الالمنيوم كمادة بلازمونية فعالة في الاطوال الموجية الممتدة من المدى تحت البنفسجي والمدى المرئي في عدة تطبيقات بلازمونية متكاملة. نستعرض في هذا البحث تاثير مادة الالمنيوم على توزيع المجال الكهرومغناطيسي لدليل موجي هجين مدمج يعمل كمدور قطبية. تمت مقارنة تاثير الالمنيوم مع مواد اخرى واسعة الاستخدام كمواد بلازمونية وهي الفضة والذهب. بالاضافة الى ذلك، تمت دراسة تاثير تصغير ابعاد المواد المستخدمة على توزيع المجال الكهرومغناطيسي في داخل الدليل الموجي الهجين وبالنتيجة على كفاءة تدوير القطبية. تم تنفيذ هذه الدراسة بناءا على نظرية العناصر المحددة باستخدام برنامج الكومسول وبطول موجي 700 نانومتر. يثبت هذا البحث كفاءة استخدام الالمنيوم كمادة بلازمونية في دوائر البواعث احادية الفوتون لانظمة توزيع المفتاح الكمي.